Surface Properties of Monolayers of Amphiphilic Poly(ethylene oxide)–Poly(styrene oxide) Block Copolymers

ARTICLE *in* THE JOURNAL OF PHYSICAL CHEMISTRY C · AUGUST 2010

Impact Factor: 4.77 · DOI: 10.1021/jp1049777

Surface Properties of Monolayers of Amphiphilic Poly(ethylene oxide)-Poly(styrene oxide) Block Copolymers

Josué Juárez,[†] Sonia Goy-López,[†] Adriana Cambón,[†] Miguel A. Valdez,[‡] Pablo Taboada,*[,†] and Víctor Mosquera[†]

Grupo de Física de Coloides y Polímeros, Departamento de Física de la Materia Condensada, Facultad de Física, Universidad de Santiago de Compostela, E-15782, Santiago de Compostela, Spain, and Departamento de Investigación en Polímeros y Materiales y Departamento de Física, Universidad de Sonora, Resales y Transversal, 83000 Hermosillo Sonora, Mexico

Received: May 31, 2010; Revised Manuscript Received: July 30, 2010

The surface properties of poly(styrene oxide)-poly(ethylene oxide) block copolymers $EO_{12}SO_{10}$, $EO_{10}SO_{10}EO_{10}$, and $EO_{137}SO_{18}EO_{137}$ at the air−water (a/w) and chloroform−water (c/w) interfaces have been analyzed by Tracker drop tensiometry, Langmuir film balance, and atomic force microscopy (AFM). The kinetic adsorptions for the block copolymer solutions at both interfaces were determined by the pendant drop technique. At the a/w, the polymer adsorption is reduced as the polymer hydrophobicity increases. Measurements of the interfacial rheological behavior of the copolymers showed that the adsorption layers at the a/w interface manifest obvious solid-like properties in the whole accessible frequency range, whereas a viscous fluid-like behavior is displayed at the c/w interface. The differences observed in the monolayer isotherms obtained for the three copolymers arose from their different hydrophobic/hydrophilic block ratios and block lengths. In this regard, copolymer $EO_{137}SO_{18}EO_{137}$ displays an adsorption isotherm with the four classical regions (pancake, mushroom, brush, and condensed states), whereas for $EO_{12}SO_{10}$ and $EO_{10}SO_{10}EO_{10}$ copolymers, only two regions were observed. The topographic images of copolymer films were obtained by AFM in noncontact mode. Surface circular micelles are observed at the two surface transfer pressures studied. A micelle size decrease and an increase in monolayer thickness are observed with an increase in transfer pressure. At the largest transfer pressure used, elongated aggregates were observed. Aggregation numbers derived from AFM pictures were in fair agreement with those obtained for micelles in solution, and they became larger as the SO weight fraction increases at a certain deposition pressure. This can be a consequence of stronger attractive interactions between the SO blocks to avoid contact with the solvent.

Introduction

Amphiphilic block copolymers are an important class of materials that have attracted considerable attention because of their outstanding solution properties, such as their self-assembly in the presence of a selective solvent or surface.[1] In particular, the interfacial properties of block copolymers have received great interest in the last years due to their role in the industrial and biological fields.[2−4] The ability of block copolymers to adsorb at an interface, modulate their properties, and even to self-assemble into well-defined nanoscale structures in two dimensions has led to their use in colloidal stability and coating processes,[5] as steric barriers at solid surfaces in medical devices to avoid undesired protein adhesion,[6] as stabilizers of liquid interfaces of foams[7] and emulsions[8] to prevent coalescence and flocculation, as templates for the rational design of large-scale nanometer architectures in thin film configurations,[9,10] and as precursors for nanoporous materials.[11]

The self-assembly behavior and physicochemical properties of diblock and triblock copolymers of polyoxyalkylenes in solution have been extensively studied.[12−21] Variation of hydrophobic monomer, block length, and architecture allows close control of their physicochemical properties. The most familiar copolymers of this type are those whose hydrophobic block is formed by units of oxypropylene ($-OCH_2CH(CH_3)$, denoted as PO), 1,2-oxybutylene ($-OCH_2CH(C_2H_5)$, denoted as BO), and oxyphenylethylene ($-OCH_2CH-(C_6H_5)$), prepared from styrene oxide (denoted as SO). These copolymers are already commercially available from BASF,[22] Dow Chemical Co.,[23] and Goldschimdt AG,[24] respectively. Nevertheless, the two-dimensional properties and aggregation of these classes of copolymers at the air/aqueous interface has been only extensively reported for poly(ethylene oxide)-poly(propylene oxide)-poly(ethylene oxide) (EO-PO-EO) block copolymers or Pluronics, the X-star shaped EO-PO-EO copolymers known as Tetronic copolymers (from BASF),[27,28] and poly(butylene oxide)-poly(ethylene oxide) block copolymers (BO-EO).[29] Very little or no report has been put into fundamentally understanding the 2-D dimensional behavior of poly(ethyelene oxide)-poly(styrene oxide) block copolymers at interfaces. Therefore, fundamental studies of SO-based block copolymers performed at either the air/water or the air/organic solvent interface can provide valuable information on their interfacial phase behavior to further guide their possible use in different biomedical and coating applications. To fill this gap, in the present work, we studied the surface behavior and surface properties of three poly(ethylene oxide)-poly(styrene oxide) block copolymers, $EO_{12}SO_{10}$, $EO_{10}SO_{10}EO_{10}$, and $EO_{137}SO_{18}EO_{137}$ (where the subscripts denote the respective block length) by dynamic

* To whom correspondence should be addressed. E-mail: pablo.taboada@usc.es. Tel: 0034981563100, ext 14042. Fax: 0034981520676.
[†] Universidad de Santiago de Compostela.
[‡] Universidad de Sonora.

10.1021/jp1049777
Published on Web 08/26/2010

TABLE 1: Molecular Characteristics of the Copolymers

	M_n[a]/g mol^{-1} (NMR)	wt % S[a] (NMR)	M_w/M_n[a] (GPC)	M_w/g mol^{-1}	cmc[b]/g dm^{-3}	$\Gamma^b_{max}/10^{-6}$ mol m^{-2}
$EO_{12}SO_{10}$	1660	73	1.05	1760	0.006	0.97
$EO_{10}SO_{10}EO_{10}$	1980	55	1.06	2130	0.012	0.91
$EO_{137}SO_{18}EO_{137}$	14 200	15	1.06	15 100	0.017	0.40

[a] Estimated uncertainty: M_n to ±3%; wt % S to ±1%, M_w/M_n to ±0.01. M_w calculated from M_n and M_w/M_n. [b] Data from ref 32 at 15 °C.

interfacial tension, dilatational rheology, Langmuir monolayers, and atomic force microscopy (AFM). The self-assembling properties and solubilization capacity of these copolymers in bulk aqueous solution were analyzed in recent studies,[30−32] in which the existence of vesicular structures (polymersomes), elongated micelles, and spherical micelles in bulk solution was reported for copolymers $EO_{12}SO_{10}$, $EO_{10}SO_{10}EO_{10}$, and $EO_{137}SO_{18}EO_{137}$, respectively. These block copolymers display different volume-to-length ratios of the hydrophobic block, relative lengths of the polyoxyethylene blocks, and polymer architectures, which enable analyzing the influence of these parameters on the block copolymer surface behavior. In this regard, due to its lengthy EO blocks and higher hydrophilicity (as denoted by its larger cmc values; see Table 1), copolymer $EO_{137}SO_{18}EO_{137}$ displays a clear and complete adsorption isotherm in which the different conformational states of the polymer chains ("pancake", "mushroom", and "brush" conformations) are observed, with a significant viscous fluid behavior and a spherical morphology of its aggregates at the surface film. In contrast, the surface pressures of $EO_{12}SO_{10}$ and $EO_{10}SO_{10}EO_{10}$ monolayers were measurable at a significantly smaller area per molecule, and only two different clear regions can be distinguished in their isotherms as a consequence of the reduction of the fractional interfacial area occupied by EO segments. In addition, copolymer $EO_{12}SO_{10}$ displays a clear rheological solid-like behavior and its organization in elongated structures similar to a string of beads upon self-assembly at the air−water (a/w) interface. Finally, a comparison of the surface behavior of these copolymers with that observed for structurally related polystyrene-poly(ethylene oxide) (PS-PEO) block copolymers is also established.[33,34]

Experimental Section

Materials. Copolymers $EO_{12}SO_{10}$, $EO_{10}SO_{10}EO_{10}$, and $EO_{137}SO_{18}EO_{137}$ were prepared by sequential oxyanionic polymerization of styrene oxide, followed by ethylene oxide, starting from a monofunctional or difunctional initiator to form the hydrophobic block as described in detail by Crothers et al.[35] Table 1 shows the molecular characteristics, critical micellar concentrations (cmc), and surface excess concentrations (Γ_{max}) of the copolymers. Water was double-distilled and degassed before used.

Dynamic Interfacial Tension and Dilatational Rheology Measurements. Pendant bubble tensiometry was used to determine the dynamic interfacial tension and the interfacial dilatational rheology at two different interfaces: air−water (a/w) and chloroform−water (c/w) interfaces. The bubble was formed at the tip of a U-shaped stainless steel needle (0.5 mm inner diameter) immersed in an aqueous block copolymer solution of the desired concentration, with the air bubble upward for the (a/w) interface, whereas downward for the (c/w) interface. Measurements were carried out in a Track tensiometer equipment (I.T. Concept, France) adapted to determine surface tension values in real time with an accuracy of ±0.1 mN/m. Interfacial tension and interfacial rheology estimations are based on the digital profile of a drop image and the resolution of the Gauss−Laplace equation. Win Drop software (I.T. Concept, France) was used to obtain the surface tension values by means of the axisymetric drop shape analysis.

The aqueous solutions concentrations of the $EO_{12}SO_{10}$, $EO_{10}SO_{10}EO_{10}$, and $EO_{137}SO_{18}EO_{137}$ block copolymers were prepared at a constant concentration of 2×10^{-3} mg/mL, below their respective cmc values. At the (a/w) interface, the analysis of the interfacial tension (γ) measurements was followed in a relative short time (2000 s) after the bubble was formed, and the dilatational elastic storage (E') and loss (E'') moduli were determined after 2000 s using a frequency sweep of 3.14, 2.09, 1.04, 0.52, 0.31, 0.15, 0.078, and 0.039 rad/s. All measurements were carried out in a time interval of 400 s using a 10% amplitude oscillation of the maximum volume drop. On the other hand, experimental data of interfacial tension, γ, at the chloroform−water interface were followed for 180 s, and after this time, volume oscillations to the stabilized pendant drop volume were applied. Storage, E', and loss, E'', moduli were determined in this way.

Briefly, the analysis of the viscoelastic properties of the absorbed layer was performed by means of a sinusoidal deformation of the drop area, A, at a defined frequency, ω, produced by the Tracker tensiometer at a time t. Calculus of the complex dilatational elasticity modulus $E(\omega)$ is determined by

$$E(\omega) = -A\frac{dy}{dA} \tag{1}$$

This can also be defined as a complex function, which can be written as

$$E(\omega) = E'(\omega) + iE''(\omega) \tag{2}$$

where E' and E'' correspond to the storage and the loss moduli, respectively, by analogy with 3-D rheology. Assuming that the mechanical properties of the adsorbed layer follow a Maxwell model behavior, the storage and loss moduli can be written as follows

$$E'(\omega) = \sum_i E_{0i}\frac{(\omega/\omega_{0i})^2}{1 + (\omega/\omega_{0i})^2} \tag{3}$$

$$E''(\omega) = \sum_i E_{0i}\frac{(\omega/\omega_{0i})}{1 + (\omega/\omega_{0i})^2} \tag{4}$$

where E_{0i} and ω_{0i} ($\omega_{0i} = 2\pi/\tau_{0i}$) are the corresponding weights of the ith relaxation element to the total elasticity modulus E_0 and the characteristic relaxation frequency, respectively; τ_{0i} is the characteristic relaxation time of the Maxwell model.

Adsorption Isotherms. Surface−pressure isotherms were recorded for monolayers spread from chloroform solutions (1 mg/mL) onto a nanopure-quality water subphase in a Langmuir−Blodgett (LB) Teflon trough (model 611 from Nima Technologies Ltc., Coventry, U.K.). Volumes ranging from 10 to 50 μL of either $EO_{12}SO_{10}$, $EO_{10}SO_{10}EO_{10}$, or $EO_{137}SO_{18}EO_{137}$ block copolymer solutions (1 mg/mL) were spread dropwise on a Millipore water subphase with a Hamilton microsyringe. To ensure complete evaporation of the solvent, a time lag of

15 min was applied between the deposition of the copolymer and the beginning of compression of the spread molecules. After chloroform was evaporated, the surface area was compressed by Teflon barriers at a rate of 5 mm·min^{-1}. The temperature was kept constant at 25 °C with a water bath, and all experiments were carried out inside a dust-free glass box. The surface pressure was measured using a Platinum Wilhelmy plate located midway between the two barriers and oriented perpendicular to them, that is, parallel to the direction of the barrier movement. The complete system was operated on an antivibration table. On the other hand, Langmuir films were transferred onto a freshly cleaved mica substrate for imaging. After spreading the chloroform solutions, again at least 15 min was allowed for solvent evaporation. The barriers were then compressed to the targeted surface pressures, 5 and 11 mN/m, respectively, at a speed of 5 mm/min. Once the targeted surface pressure was reached and stable, the cleaved mica was lifted up at a speed of 1 mm/min. Film transfer ratios of 0.95−1.0 were obtained. The resulting films were individually stored at room temperature in clean closed vials.

Atomic Force Microscopy. AFM images of block copolymer monolayers were performed on freshly cleaved mica substrates. The measurements were performed in a JEOL instrument (model JSPM 4210) in noncontact mode using nitride cantilevers NSC15 from MicroMasch, U.S.A. (typical working frequency and spring constant of 325 kHz and 40 N/m, respectively). The AFM samples were dried in air or under a nitrogen flow when required. Control samples (freshly cleaved mica and buffer solution) were also investigated to exclude possible artifacts. Topography and phase-shift data were collected in the trace and retrace direction of the raster, respectively. The offset point was adapted accordingly to the roughness of the sample. The scan size was usually 500 nm (aspect ratio, 1 × 1), with a sample line of 256 points and a step size of 1 μm. The scan rate was tuned proportionally to the area scanned and kept within the 0.35−2 Hz range. Each sample was imaged several times at different locations on the substrate to ensure reproducibility. In all cases, the imaging of LB films was performed far from the edge of the glass substrate to minimize local effects caused by turbulent water flow at the boundary and meniscus effects during transfer. Diameters and heights of copolymer aggregates were determined by sectional analysis taken from the average of several sections through the aggregates.

Results and Discussion

Some molecular characteristics of the investigated block copolymers $EO_{12}SO_{10}$, $EO_{10}SO_{10}EO_{10}$, and $EO_{137}SO_{18}EO_{137}$ are shown in Table 1. As expected, the two triblock copolymers have higher cmc values than the diblock. This effect originates from the entropy of the triblock chains constrained by two block junctions in the core−shell interface of the micelle compared to the only constrain for the diblock chain. The copolymers were chosen to form two pairs, one with similar-sized hydrophobic SO blocks but different polymer architectures ($EO_{12}SO_{10}$ and $EO_{10}SO_{10}EO_{10}$) and the other with completely different hydrophilic EO block lengths ($EO_{10}SO_{10}EO_{10}$ and $EO_{137}SO_{18}EO_{137}$) and relatively similar hydrophobic SO blocks. This was made with the purpose of comparing the relative importance of the polymer architecture and the hydrophilic/hydrophobic block ratio on both polymer adsorption and surface rheological behavior at the air/water and chloroform/water interfaces. In previous studies, the polymer architecture, the volume-to-length ratios of the hydrophobic block, and the relative lengths of the polyoxyethylene blocks were found to be helpful in controlling the micellar morphology of these copolymers.[32,36] In particular, the coexistence of spherical micelles with vesicles (polymersomes) was observed for copolymer $EO_{12}SO_{10}$; in contrast, the formation of elongated and spherical micelles for copolymers $EO_{10}SO_{10}EO_{10}$ and $EO_{137}SO_{18}EO_{137}$, respectively, was found upon their self-assembly.[32]

Dynamic Surface Tension

The surface tension of the copolymers as a function of time for copolymers $EO_{12}SO_{10}$, $EO_{10}SO_{10}EO_{10}$, and $EO_{137}SO_{18}EO_{137}$ at a concentration of 2×10^{-3} mg/mL is illustrated in Figure 1. The low concentration used allowed us to work in relative short time intervals to achieve a quasi-stabilization at both air−water (a/w) and chloroform−water (c/w) interfaces, and it also avoided complications associated with chloroform evaporation. Nevertheless, the true equilibrium state was not attained for any of the copolymers within 1 h of adsorption because the surface tension still continued to decrease slightly with time.

Usually, the dynamic surface tension curves can be divided in three stages: At relative low polymer concentrations, a quasi-plateau or a very slow decrease of $\gamma(t)$ can be distinguished at short times, which corresponds to the so-called lag phase. The postlag phase stage of the polymer adsorption process is characterized by a rapid decrease of $\gamma(t)$, which is associated with the increased number of copolymer molecules adsorbed at the interface and to conformational changes of the polymer chains adsorbed at the interface. In this stage, lateral interactions between adsorbed macromolecules stabilize the monolayer and the adsorption of the molecules continues to be controlled by macromolecule diffusion without appreciable desorption. Finally, the postlag stage transforms to the final (or last) adsorption phase, which is recognized by some slowing down of the interfacial tension decrease rate. At this stage, the dense adsorption layer exerts electrostatic and steric repulsion toward newly arrived macromolecules and hinders their adsorption at the interface.[37,38] Nevertheless, despite their hindrance, the interfacial tension tends to continuously decrease during this stage because of the high surface activity of the block copolymers.

In our case, initial γ values of 66.4, 64.5, and 57.1 mN/m were observed for copolymers $EO_{12}SO_{10}$, $EO_{10}SO_{10}EO_{10}$, and $EO_{137}SO_{18}EO_{137}$, respectively (see Figure 1a), as a consequence of the very rapid migration of copolymer molecules from the bulk solution to the a/w interface, giving rise to a block copolymer monolayer. For copolymer $EO_{137}SO_{18}EO_{137}$, we assume that the observed experimental data corresponds to the last part of the postlag time stage and the final polymeric adsorption stage. In contrast, for both $EO_{12}SO_{10}$ and $EO_{10}SO_{10}EO_{10}$, the curve profile can be divided in three stages after an almost instantaneous surface tension decrease. We will keep the same nomenclature (lag phase, postlag phase, and final adsorption phase) to define the regions in these curves despite that their true meaning corresponds to values departing from the surface tension value of pure water. For copolymer $EO_{12}SO_{10}$, the lag phase is longer, and the decrease of γ in the postlag phase is faster than for copolymer $EO_{10}SO_{10}EO_{10}$, probably as a result of its greater hydrophobicity. Similarly, a much larger EO block for copolymer $EO_{137}SO_{18}EO_{137}$ if compared to $EO_{10}SO_{10}EO_{10}$ results in a larger surface tension decrease in the very early stages of the adsorption process, which we attribute to an increased repulsion between the EO chains, giving rise to an enhancement of the surface pressure.

If the adsorption kinetics is controlled by the diffusion of macromolecules from the bulk solution to the interface, for

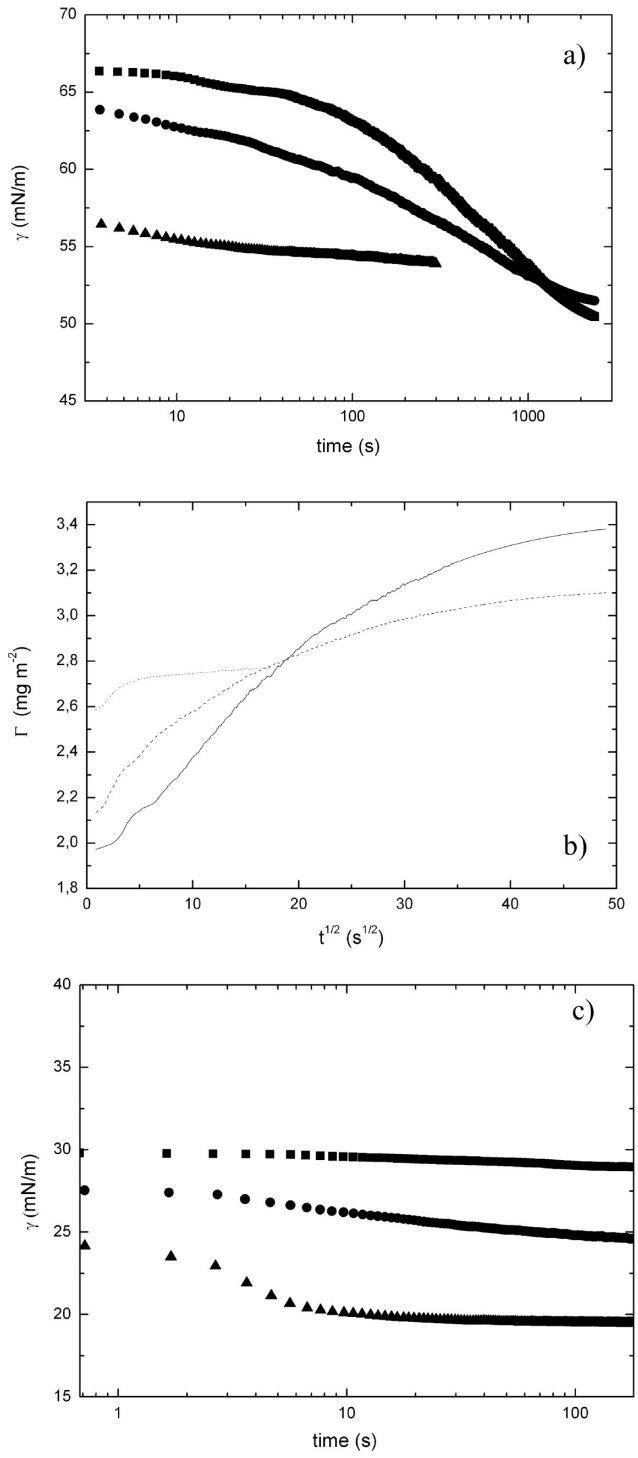

Figure 1. (a) Variation of surface tension, γ, with time at the air−water interface for copolymers (○) $EO_{12}SO_{10}$, (●) $EO_{10}SO_{10}EO_{10}$, and (▲) $EO_{137}SO_{18}EO_{137}$. (b) Variation of surface concentration, Γ, with time at the air−water interface for copolymers (—) $EO_{12}SO_{10}$, (•••••) $EO_{10}SO_{10}EO_{10}$, and (----) $EO_{137}SO_{18}EO_{137}$. (c) Variation of surface tension, γ, with time at the chloroform−water interface for copolymers (■) $EO_{12}SO_{10}$, (●) $EO_{10}SO_{10}EO_{10}$, and (▲) $EO_{137}SO_{18}EO_{137}$.

strongly adsorbing species, this is described by the Ward−Torday equation,[39] $\Gamma(t) = 2c_0(Dt/\pi)^{1/2}$, where c_0 is the polymer concentration and D the bulk diffusion coefficient. A diffusion-controlled adsorption mechanism will be expected to give a straight line in a plot of Γ versus $t^{1/2}$. In these experiments, the direct connection between Γ and t cannot be measured, but a measured value of Π may be converted to a relative value of Γ by using the scaling expression $\Pi \sim \Gamma^y$ and the calculated value of y from the adsorption isotherm experiments (see below). Figure 1b shows such a plot for the three copolymers. The proportionally constant was set equal to 1 $(m^2 \cdot mg^{-2})^y$ $mN \cdot m^{-1}$, which implies that the surface pressure is set to 1 $mN \cdot m^{-1}$ at a surface concentration of 1 $mg \cdot m^{-2}$. This value is typical for that found for many polymers.[40,41] From this figure, it can be observed that the expected straight line is quite steep at very short times, but a curvature in the plot is present at larger times. This may indicate that the diffusion-controlled adsorption process only operates during the first few seconds of the process and, then, is more likely controlled by a slow configurational change and reorientation of the polymer molecules at the surface. At this respect, a bimodal type of adsorption kinetics of Pluronic block copolymers, including initial diffusion, followed by an internal reorganization of the structure, was discussed recently.[42]

On the other hand, there was no measurable effect on the interfacial tension at the chloroform/water interface (c/w) due to the adsorption of copolymer $EO_{12}SO_{10}$ (see Figure 1c). This behavior might originate from the small amount of copolymer at the interface due to the slow diffusion of their chains to the interface in combination with a low bulk concentration. The slow diffusion can be associated with the fact that chloroform is a good solvent for both EO and SO blocks, and provided that copolymer $EO_{12}SO_{10}$ is very hydrophobic, the copolymer chains prefer being in the organic phase. This can be additionally corroborated with the progressively faster decrease observed in surface tension values at short times for the increasingly hydrophilic copolymers $EO_{10}SO_{10}EO_{10}$ and $EO_{137}SO_{18}EO_{137}$. This faster decrease also enables the development of a postlag phase for these copolymers. In fact, for the latter copolymer, the curve profile is very similar to that obtained at the a/w interface, although the absolute γ values are quite different as a result of the depression of interfacial tension due to the presence of chloroform.

Dilatational Rheology. Analysis of the frequency dependence of the dilational moduli allows us to get detailed information about the type of interactions existing between polymer chains located at the interface. Figure 2 shows the frequency dependence of storage, E', and loss, E'', dilatational moduli in semilogarithmic plots for the adsorbed layers of block copolymers $EO_{12}SO_{10}$, $EO_{10}SO_{10}EO_{10}$, and $EO_{137}SO_{18}EO_{137}$ at both the a/w and the c/w interfaces. The frequency dependence of both E' and E'' is generally believed to be caused by relaxation processes at the interface.[43,44] A satisfactory rheological description of the adsorption layers of macromolecules may be done by considering several characteristic relaxation frequencies (or relaxation times, τ), which are related to the adsorption−desorption exchange of polymer chains between the surface and the adjacent subinterface layer during dilatational perturbation and molecular reconformation of the adsorbed layer.[38] In this way, the frequency dependences of storage (E') and loss (E'') moduli were fitted to the sum of two Maxwell elements

$$E'(\omega) = E_{01}\frac{(\omega/\omega_{01})^2}{1 + (\omega/\omega_{01})^2} + E_{02}\frac{(\omega/\omega_{02})^2}{1 + (\omega/\omega_{02})^2} \quad (5)$$

$$E''(\omega) = E_{01}\frac{(\omega/\omega_{01})}{1 + (\omega/\omega_{01})^2} + E_{02}\frac{(\omega/\omega_{02})}{1 + (\omega/\omega_{02})^2} \quad (6)$$

where E' is related to lateral interactions between polymer segments at the interface plane and is relevant for the rigidity of interfacial film, whereas E'' is related to molecular reorga-

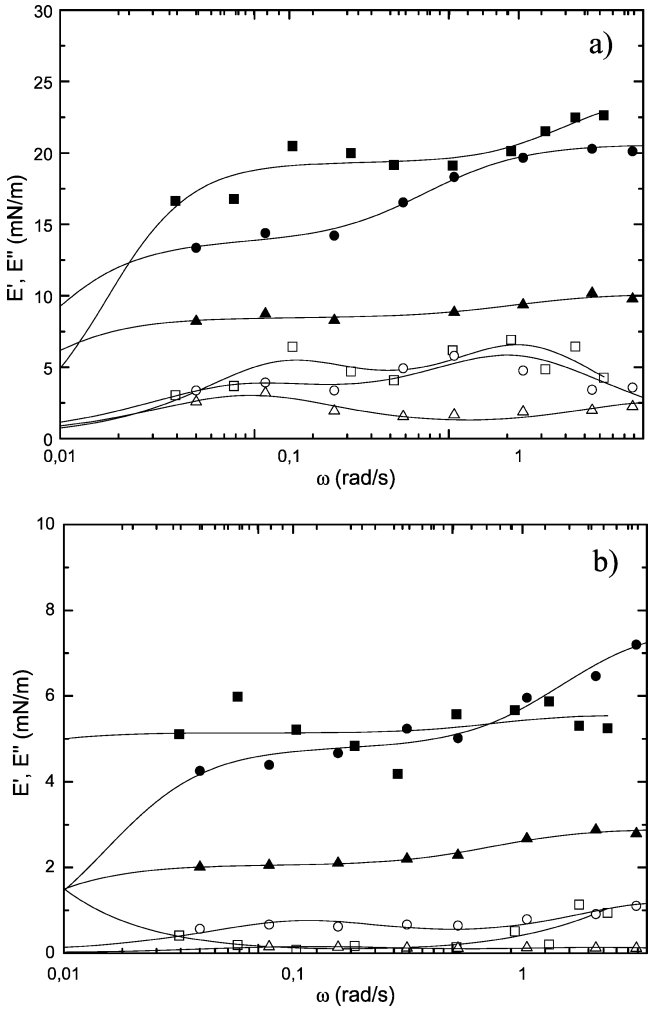

Figure 2. Storage, E' (closed symbols), and loss, E'' (open symbols), moduli as a function of frequency for copolymers (■) $EO_{12}SO_{10}$, (●) $EO_{10}SO_{10}EO_{10}$, and (▲) $EO_{137}SO_{18}EO_{137}$ at the (a) air−water and (b) chloroform−water interfaces.

nization processes, such as the expulsion of polymer chains from the interface upon compression and the interactions of polymer molecules with adjacent liquid molecules.[45] The first characteristic relaxation time, τ_{01}, is usually attributed to the adsorption−desorption exhange of molecules and polymer segments between the surface and the adjacent subsurface layer during dilatational perturbations of the interface; τ_{02} corresponds to slower reconformations of the adsorbed macromolecules inside the adsorption layer.

At the a/w interface, the adsorption layers manifest obvious solid-like properties in the whole accessible frequency range ($\omega = 0.039-3.14$ rad/s) with $E' > E''$, following the sequence $EO_{12}SO_{10} > EO_{10}SO_{10}EO_{10} > EO_{137}SO_{18}EO_{137}$, and with a low significance of dissipative processes during dilational deformations of these block copolymer layers. These values suggest a more fluid layer in the case of copolymer $EO_{137}SO_{18}EO_{137}$ as a consequence of its lower hydrophobicity (larger cmc) due to the presence of extended oxyethyelene chains. In contrast, copolymer $EO_{12}SO_{10}$ shows the most important solid-like behavior, which involves the formation of tightly packed copolymer chains at the interface to avoid contact between hydrophobic blocks and water. Molar copolymer concentration differences slightly affect the final dilatational moduli values (not shown). We also point out that the storage modulus E' slightly, but continuously, increases with frequency, whereas

TABLE 2: Characteristic Relaxation Times, τ_{01} and τ_{02}, and Characteristic Dilatational Moduli Weights of Each Relaxation Mode, E_{01} and E_{02}, of Copolymers $EO_{12}SO_{10}$, $EO_{10}SO_{10}EO_{10}$, and $EO_{137}SO_{18}EO_{137}$ at the Air−Water and Chloroform−Water Interfaces

	τ_{01}[a]/s	τ_{02}[a]/s	E_{01}[a]/mN m^{-1}	E_{02}[a]/mN m^{-1}
		air−water		
$EO_{12}SO_{10}$	3.2	48.0	4.9	19.3
$EO_{10}SO_{10}EO_{10}$	10.0	75.0	6.8	13.8
$EO_{137}SO_{18}EO_{137}$	6.6	81.1	1.7	8.5
		chloroform−water		
$EO_{12}SO_{10}$	56.3	5.7	5.6	0.3
$EO_{10}SO_{10}EO_{10}$	51.1	8.7	4.8	2.4
$EO_{137}SO_{18}EO_{137}$	75.9	7.1	2.1	0.9

[a] Estimated uncertainty: τ_{01}, τ_{01} to ±1%; E_{01}, E_{02} to ±0.01.

the loss modulus E'' is close to zero, in particular, for copolymer $EO_{137}SO_{18}EO_{137}$. This involves that the exchange processes between the surface layer and bulk solution are relatively important, and as the frequency becomes larger, the system does not have enough time to reach the equilibrium and returns most of the stored energy. Thus, the elasticity becomes larger. Otherwise, the time is not long enough to modify the interfacial concentration gradient through different relaxation processes at high oscillation frequencies. As a result, the dilational moduli increase with increasing oscillation frequencies. On the other hand, τ_{01} and τ_{02} values at the a/w interface for copolymers $EO_{12}SO_{10}$, $EO_{10}SO_{10}EO_{10}$, and $EO_{137}SO_{18}EO_{137}$ derived from the Maxwell modelization are displayed in Table 2. In particular, copolymer $EO_{12}SO_{10}$ possesses the shortest relaxation times τ_{01} and τ_{02}, which indicates the fastest adsorption−desorption exchange and a rapid molecular reorganization of the polymer chains adsorbed at the interface probably as a result of its lower molecular weight, diblock architecture, and larger hydrophobicity.

At the c/w interface, the profiles of the dilational rheology curves display similar behavior as at the a/w interface, although the absolute values of E_{01} and E_{02} are sensibly lower, particularly the former ones. For this reason, it seems that a viscous fluid-like behavior is displayed by the three copolymers at the c/w interface. Moreover, the values obtained for the characteristic relaxation times τ_{01} and intrinsic elasticity E_{01} decreased, whereas τ_{02} and E_{02} increased if compared to those obtained at the a/w interface; that is, a reverse behavior is found. This may point out that the copolymers have been weakly adsorbed at the c/w interface because copolymer molecules tend to stay at the chloroform phase because chloroform is a good solvent for both hydrophilic and hydrophobic copolymer blocks, as previously mentioned.

Adsorption Isotherms. Monolayers of $EO_{12}SO_{10}$, $EO_{10}SO_{10}EO_{10}$, and $EO_{137}SO_{18}EO_{137}$ block copolymers were spread on a Langmuir−Blodgett trough balance, and the $\Pi-A$ isotherms were obtained (see Figure 3a). In the present study, copolymer $EO_{137}SO_{18}EO_{137}$ displays a classical isotherm pattern divided in four regions. When no pressure is exerted, copolymer chains should lie on the interface with a flat ("pancake") conformation parallel to the surface plane.[46,47] The area occupied is a function of the number of SO and EO units. Roughly, the maximum cross-sectional area occupied by an EO unit is 13−16.5 Å^2[25] and that occupied by an SO unit can be taken similar as that of a PS unit (50 Å^2).[48] Once hydrated, the areas of EO and SO units increase by 8.5 Å^2 (a water molecule). Once the compression of the $EO_{137}SO_{18}EO_{137}$ monolayer began, the surface pressure gradually increased until reaching an area under compression of 7350 Å^2/molecule. This value agrees with the

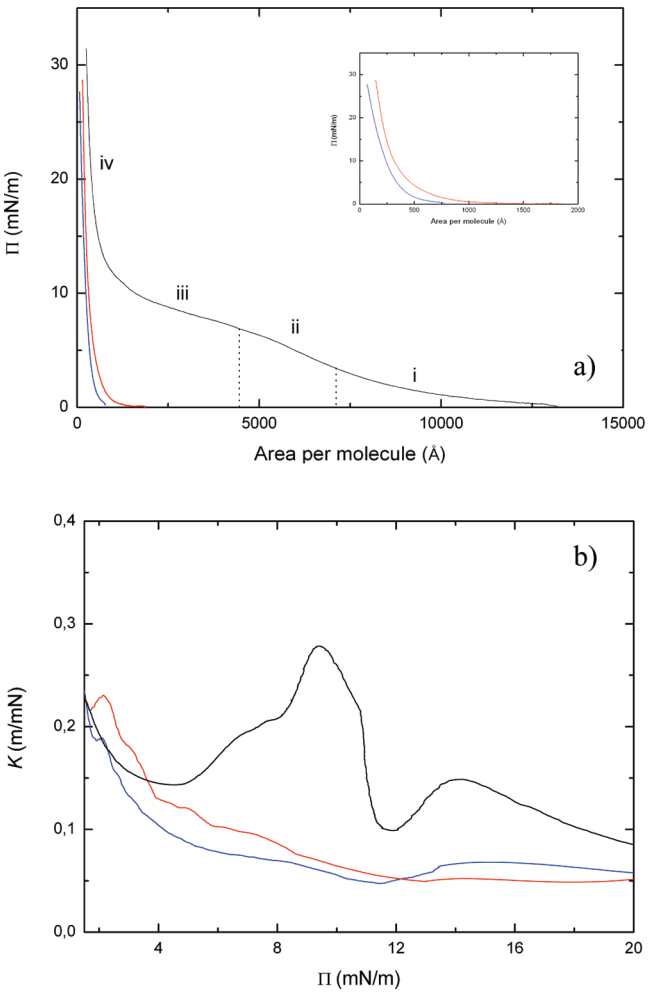

Figure 3. (a) Surface pressure, Π, isotherms for spread monolayers of copolymers (blue line) $EO_{12}SO_{10}$, (red line) $EO_{10}SO_{10}EO_{10}$, and (black line) $EO_{137}SO_{18}EO_{137}$. The inset is an enlargement of the isotherm corresponding to copolymers $EO_{12}SO_{10}$ and $EO_{10}SO_{10}EO_{10}$. (b) Compressibility, K, against surface pressure of spread monolayers of copolymers (red line) $EO_{12}SO_{10}$, (blue line) $EO_{10}SO_{10}EO_{10}$, and (black line) $EO_{137}SO_{18}EO_{137}$.

sum of the maximum transverse area occupied by all EO and SO units of copolymer $EO_{137}SO_{18}EO_{137}$. As the pressure increased, the hydrophobic SO blocks, initially on the air−water interface, were lifted away. The surface pressure at which this phenomenon occurs is usually very low owing to the weakness of the interaction between the aqueous medium and the hydrophobic groups[49] (Figure 3a, region ii). The 4800 Å^2/molecule area corresponds to an arrangement of the molecules that leads to an occupied area 35% lower than the original value. From 6.1 to 9.8 mN/m, another region of a lower slope appears due to a change in the copolymer conformation, which enables the penetration of the hydrophilic EO chains into the subphase: the copolymer adopts a "mushroom" conformation (Figure 3a, region iii). In this region, there is a slight increase in the surface pressure as the surface area is decreased, indicating that a true first-order transition does not occur. This "pseudoplateau" is interpreted as a rearrangement of the SO coils into "loops" within the monolayer regime and the immersion of more EO units in the aqueous subphase. The end of the pseudoplateau region correponds to an area of ∼1800 Å^2/molecule, which indicates that the vast majority of EO units is in the subphase. Isotherms of PS-PEO copolymers of different PEO lengths showed that the PEO block length largely influences in the character of this transition.[50] Further compression causes a rapid increase in surface pressure. Block copolymer molecules gradually become closer, the mobility of the blocks becomes restricted because of both space limitations and the increase in lateral interactions, and the copolymer molecules reorganize into a "brush conformation" (Figure 3a, region iv).[51−53] In the subphase, the EO chains entangle with neighboring copolymer molecules, whereas at the interface, the SO blocks can form loops and even are partially solubilized in the aqueous EO layer. If the area is further restricted, both hydrophilic and hydrophobic blocks become stretched (condensed state).[25] The extrapolation of the experimental data above this pressure indicates that the area occupied per molecule at the condensed state (A_L) is 276 Å^2.

In contrast, copolymers $EO_{12}SO_{10}$ and $EO_{10}SO_{10}EO_{10}$ exerted a relatively low resistance to compression at the largest and medium areas per molecule of their isotherms (see Figure 3a), as expected from their low molecular weight, shorter SO and EO segments, and fair aqueous solubility at low concentrations. The surface pressures of $EO_{12}SO_{10}$ and $EO_{10}SO_{10}EO_{10}$ monolayers were measurable at significantly smaller areas per molecule than for the $EO_{137}SO_{18}EO_{137}$ monolayer. Only two well-defined regions can be distinguished in their isotherms. When the area per molecule is large, the surface pressure slowly increases as the area decreases. Above 1 and 2 mN/m for $EO_{12}SO_{10}$ and $EO_{10}SO_{10}EO_{10}$, respectively, a very slight pseudoplateau might be depicted. This behavior arises from the increasing weight fraction of SO blocks at the interface, which reduces the fractional interfacial area occupied by EO segments. Above 3 and 5 mN/m, respectively, a sharp rise in the surface pressure occurs. This is consistent with a significant contribution from the SO domains, showing no plateau or pseudoplateau at 10 mN/m. In fact, the monolayers of both block copolymers can be considered as condensed-like films in comparison with that obtained for $EO_{137}SO_{18}EO_{137}$, which behaves as an expanded-like film.[53] The area occupied per molecule at the condensed state (A_L) is 167 Å^2 for $E_{12}S_{10}$ and 135 Å^2 for $EO_{10}SO_{10}EO_{10}$, respectively. These values are in fair agreement with the areas predicted from the number of SO units of $EO_{12}SO_{10}$ and $EO_{10}SO_{10}EO_{10}$, respectively, and support the fact that the interface is occupied only by SO blocks. This is also confirmed by the fact that, despite that the isotherms of the copolymers clearly differ in their shape at low surface pressures, they merge, becoming almost superimposable at large surface pressures.

On the other hand, the compressibility modulus ($K = -1/A \times (dA/d\pi)$) displays local maxima for every phase transition in the copolymers' monolayers. As shown in Figure 3b, several phase transitions located at ∼6.5, ∼9.5, and ∼14.0 m/Nm were found for copolymer $EO_{137}SO_{18}EO_{137}$. Those at ∼6.5 and ∼9.5 m/Nm are PEO-related phase transitions, which are a consequence of the penetration of PEO chains in the subphase, leaving the air−water interface to form a swollen three-dimensional structure in the aqueous phase (in particular, at ∼9.5 m/mN). After the latter peak, the subsequent minimum and additional maximum found at larger surface pressures is a result of the increasing repulsion between SO segments in the top layer and PEO segments in the subphase. This facilitates the desorption of SO blocks due to enhanced repulsions within the layer and the formation of loops and tails, which leads to a faster redistribution between the upper and lower regions of the layer. On the other hand, only slight maxima at ∼2.0 m/mN and a shoulder at ca. 6.0 m/mN are found for copolymers $EO_{12}SO_{10}$ and $EO_{10}SO_{10}EO_{10}$. The maximum can be related to a PEO phase transition, whereas the shoulder at 6.5 m/mN can resemble

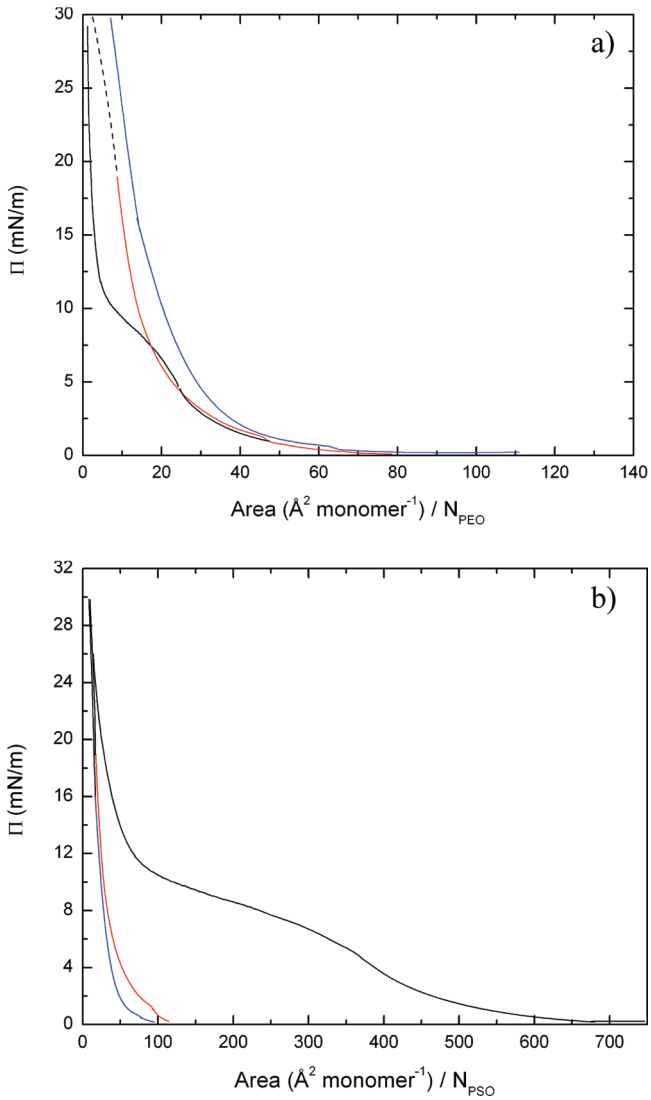

Figure 4. Surface pressure isotherms plotted with respect to (a) the average area per EO repeat unit and (b) the average area per SO repeat unit for copolymers (blue line) $EO_{12}SO_{10}$, (red line) $EO_{10}SO_{10}EO_{10}$, and (black line) $EO_{137}SO_{18}EO_{137}$.

some kind of structural rearrangement of SO blocks before complete film condensation. The absence of the transition at 9.5 m/Nm for both $EO_{12}SO_{10}$ and $EO_{10}SO_{10}EO_{10}$ is a consequence of their small PEO block length.

The effect of the polymer structure can be easily visualized by plotting the surface pressure as a function of the average surface area per monomer. Isotherms plotted with the molecular area normalized with respect to the number of EO and SO segments are shown in Figure 4a,b. Figure 4a demonstrates that all of the isotherms of the three copolymers fall on a single curve for surface areas corresponding to the semidilute regime. This indicates that the isotherm in this regime is mainly dependent on the EO block length. Beyond the pseudoplateau, all copolymers appear to be affected by the SO/EO ratio. In the semidilute regime, the Flory coefficient of the system can be obtained from the des Cloizeaux equation,[54] which describes the relationship between the surface pressure and the surface concentration (Γ) of a polymer by

$$\Pi = CA^{-y} = K\Gamma^{y} \text{ with } y = d\nu/(d\nu - 1) \qquad (7)$$

where C and K are proportionality constants, A is the molecular area, y is the scaling exponent, d is the geometrical dimension, and ν is the Flory coefficient used to express the radius of gyration in terms of molecular weight ($R_g \approx M^{\nu}$) and is a measure of the solvent quality.[55] For chains in good solvent conditions, the exponent ν is theoretically predicted to be 0.75 for a 2D self-avoiding walk and 0.6 for a 3D self-avoiding walk. Consequently, the theoretical exponent for the scaling of the surface pressure with the area per molecule is $y = 3$ for the 2D semidilute regime and $y = 2.25$ for the 3D semidilute regime. Plotting the variation of the surface pressure Π versus the inverse of the area per molecules $1/A$ on a double-logarithmic scale for the three different copolymers in the intermediate region between the dilute regime and the plateau, we have obtained y exponents of 2.28, 2.37, and 2.54 for $EO_{12}SO_{10}$, $EO_{10}SO_{10}EO_{10}$, and $EO_{137}SO_{18}EO_{137}$, respectively. This indicates that the chain conformation is almost a 3D interpenetrated layer for copolymers $EO_{12}SO_{10}$ and $EO_{10}SO_{10}EO_{10}$ and a intermediate between a purely 2D entangled layer and a 3D interpenetrated layer for copolymer $EO_{137}SO_{18}EO_{137}$, as also observed for different PSO-EO block copolymers.[56] From Figure 4b, the isotherms superimposed in the concentrated regime for the three block copolymers, which denotes that the isotherm shape is now determined by the SO chain length and SO/EO molar ratio.

Summarizing, if the SO block is short compared with the EO block, as in the case of copolymer $EO_{137}SO_{18}EO_{137}$, its role is limited to anchoring the EO chains at the air−water interface and it has no influence on the surface pressure isotherm or on the segment profile of the EO chains normal to the interface. But, as the SO block is repulsive to the EO block, as in the case of $EO_{12}SO_{10}$ and $EO_{10}SO_{10}EO_{10}$, this should modify the attractive nature of the interface for the EO and, therefore, the expected concentration profile for the EO chains, as also occurred for PS-EO and EO-PS-EO copolymers[34,47,49,57,58] and Pluronics[26] and Tetronics (four star-shaped ethylene oxide-propylene oxide block copolymers).[28] The balance between these opposite interactions will depend on the copolymer surface density, the SO block length, and the temperature.

AFM. Besides the isotherm data, detailed insight into the organization and morphology of the Langmuir−Blodgett monolayers should rely on the images of their corresponding films by AFM. We compare the morphologies of the three samples deposited at different pressures. Figure 5 shows AFM images of the block copolymer films on freshly cleaved mica obtained at 5 and 11 mN/m surface pressures. Aggregation was observed for all the copolymers investigated. The surface micelle assembly can take place (i) during the solvent evaporation step or (ii) during the LB tranfer. Nevertheless, dynamic light-scattering measurements (DLS, data not shown) of the three copolymers in chloroform did not show any evidence of micelle formation, which implies that the formation of EO-SO surface features in LB films are the result of spontaneous copolymer aggregation at the air−water interface rather than a transfer of micelles formed in the spreading solution.[59]

At a surface pressure of 5 mN/m, the AFM images of the block copolymers $EO_{12}SO_{10}$, $EO_{10}SO_{10}EO_{10}$, and $EO_{137}SO_{18}EO_{137}$ show the presence of spherical aggregates with diameters of 6.7 ± 0.4, 7.9 ± 0.2, and 9.1 ± 0.3 nm, respectively (Figure 5a,c,e; see Figure S1 in the Supporting Information for size distributions). The average height of the aggregates obtained at this surface pressure is 2.03 ± 0.01, 1.25 ± 0.01, and 1.52 ± 0.01 nm for $EO_{12}SO_{10}$, $EO_{10}SO_{10}EO_{10}$, and $EO_{137}SO_{18}EO_{137}$, respectively, so they can be identified as dots or circular micelles (see Figure 6 as an example and Figure S2 in the Supporting Informationfor height distributions). The difference in dot heights for the three copolymers is a consequence of the

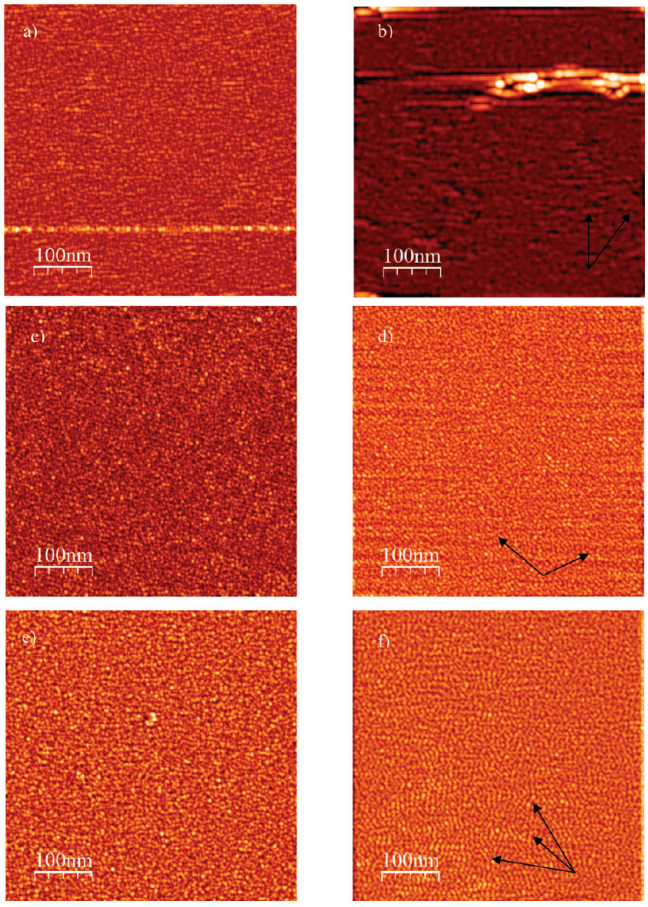

Figure 5. Typical AFM images of Langmuir−Blodgett films of the copolymers $EO_{12}SO_{10}$ (a, b), $EO_{137}SO_{18}EO_{137}$ (c, d), and $EO_{10}SO_{10}EO_{10}$ (e, f) at transfer surface pressures of 5 and 11 mN/m, respectively. Arrows denote some elongated polymer structures.

copolymer hydrophobicity and SO/EO ratio: Assuming that the length of an SO unit is 0.18 nm per chain unit,[60] the average length of the fully stretched SO_{10} and SO_{18} blocks would be 1.8 and 3.3 nm. As the central block is looped in the aggregate core in the case of the triblock copolymers, the effective length would be 0.9 and 1.7 nm, respectively. On comparison with the experimental values, the SO blocks of copolymers $EO_{12}SO_{10}$ and $EO_{10}SO_{10}EO_{10}$ display a more extended perpendicular configuration on the water surface ("brush" state) than for copolymer $EO_{137}SO_{18}EO_{137}$, for which a "mushroom" conformation is predominant, confirming the surface−pressure isotherm data.

When the transfer surface pressure rises to 11 mN/m, the height of the $EO_{12}SO_{10}$ layer largely increases up to 5.2 ± 0.01 nm, which suggests the formation of multilayers at the a/w interface. Formation of large aggregates is also observed as a consequence of micelle association. Part of these supra-aggregates display an elongated morphology, which seems to be composed of a string of beads, the beads being circular micelles in contact each other. Similar necklace-network strctures have been observed, for example, in Langmuir−Blodgett films of mixed PS and PS-P2VP (P2VP, poly(2-vinylpyridine)).[61] This large-scale aggregation pattern is observed, suggesting the possibility of a dewetting process, although we cannot neglect the possible influence of particle aggregation upon film drying. In the case of copolymers $EO_{10}SO_{10}EO_{10}$ and $EO_{137}SO_{18}EO_{137}$, the increase in film thickness increase upon transfer at 11 mN/m is less pronounced, with mean height values of 1.95 ± 0.01 and 3.90 ± 0.02 nm, respectively. These values point out that the SO blocks of both copolymers are in a full extended perpendicular configuration (brush state) at this transfer surface pressure. The average size of the aggregates is 7.2 ± 0.1, 5.6 ± 0.3, and 7.3 ± 0.1 nm for $EO_{12}SO_{10}$, $EO_{10}SO_{10}EO_{10}$, and $EO_{137}SO_{18}EO_{137}$, respectively, at this transfer pressure. Comparing these values with those measured at a surface pressure of 5 mN/m, we can assume that a compaction of the aggregates formed by copolymers $EO_{10}SO_{10}EO_{10}$ and $EO_{137}SO_{18}EO_{137}$ has occurred in order to accommodate all copolymer chains at the interface. Moreover, formation of elongated micelles is also observed at 11 mN/m for the former copolymers (see Figure 5d,f). In fact, elongated micelles in bulk solution have been previously found for copolymer $EO_{10}SO_{10}EO_{10}$, whereas for $EO_{137}SO_{18}EO_{137}$, only spherical micelles were detected.[32]

In contrast to what was found by Deveraux et al.[60] and Moffitt et al.[33] for PS-EO block copolymers, the deposition pressure influences the structure of the resulting copolymer surface aggregates. Furthermore, PS-EO copolymers show additional surface structures other than dots (elongated structures, lamellae...) when the EO weight contents are lower than 12%;[33] however, for SO-based copolymers, elongated structures are

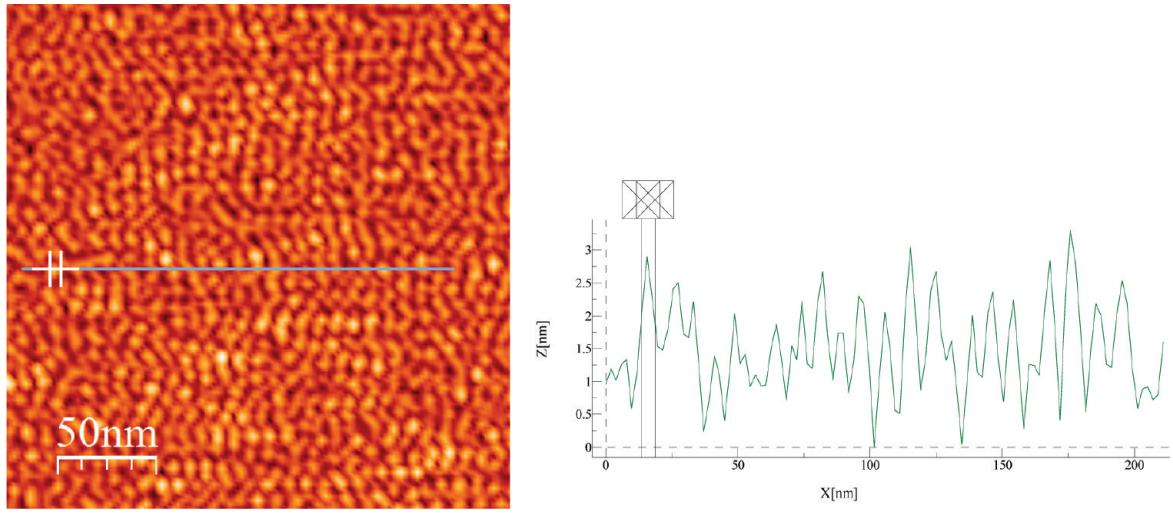

Figure 6. Determination of micelle size for copolymer $EO_{137}SO_{18}EO_{137}$ at a surface pressure of 11 mN/m through sectional analysis. *X* represents the aggregate diameter and *Z* the aggregate height.

TABLE 3: Aggregate Number, N_{agg}, for Surface Micelles of Copolymers $EO_{12}SO_{10}$, $EO_{10}SO_{10}EO_{10}$, and $EO_{137}SO_{18}EO_{137}$

	N_{agg}	
	5 mN/m	11 mN/m
$EO_{12}SO_{10}$	40	144
$EO_{10}SO_{10}EO_{10}$	29	68
$EO_{137}SO_{18}EO_{137}$	10	36

already observed at an EO content of 27% for copolymer $EO_{12}SO_{10}$. The lower glass transition temperature of SO (~40 °C) compared with that of a PS (~100 °C), which is thought to be associated with plasticization of water molecules associated with the ether oxygen of the SO units,[12] might involve a larger mobility of SO blocks in the aggregates, thus enabling a certain restructurization of the aggregates consisting of lateral interactions between SO segments of adjacent circular aggregates.

The aggregation number (N_{agg}) of the copolymer aggregates was evaluated from the AFM images in conjuction with the $\Pi-A$ isotherms. N_{agg} was determined by dividing the number of micelles per unit area by the molecular area from the $\Pi-A$ isotherms at the corresponding transfer pressure. The height profile of the micelles was generally found to be hemispheric with the condition used to scan the samples. From Table 3, it can be seen that N_{agg} increases with the increase of the SO weight fraction at a certain deposition pressure, which can be a consequence of stronger attractive interactions between the SO blocks to avoid contact with the solvent. Values of N_{agg} are in fair agreement with those obtained for micelles in solution.[32] The lower aggregation number of copolymer $EO_{137}SO_{18}EO_{137}$ may arise from the steric repulsion of EO chains at the interface due to the longer PEO blocks if compared to the other block copolymer. Moreover, N_{agg} for the corresponding samples tends to increase with the increase of the deposition pressure because further compression will provide enough energy to overcome repulsion between EO segments and form larger aggregates.

Conclusions

In summary, the spontaneous adsorption of block copolymers $EO_{12}SO_{10}$, $EO_{10}SO_{10}EO_{10}$, and $EO_{137}SO_{18}EO_{137}$ at the air−water interface is observed to be slowed down when the hydrophobicity of the molecule is increased. In contrast, at the chloroform−water interface, no measurable effect is observed for copolymer $EO_{12}SO_{10}$ due to the slow diffusion of its chains to the interface in combination with a low bulk concentration, the slow diffusion associated with the fact that chloroform is a good solvent for both EO and SO blocks. In addition, the adsorption layers at the a/w interface manifest obvious solid-like properties in the whole accessible frequency range with $E' > E''$, following the sequence $EO_{12}SO_{10} > EO_{10}SO_{10}EO_{10} > EO_{137}SO_{18}EO_{137}$, and with a low significance of dissipative processes. In contrast, a viscous fluid-like behavior is displayed by the three copolymers at the c/w interface. Copolymer $EO_{137}SO_{18}EO_{137}$ displays an adsorption isotherm with the four classical regions representing pancake, mushroom, brush, and condensed states, with the presence of a pseudoplateau attributed to the pancake-to-brush transition as EO chains submerge into the aqueous subphase. On the other hand, for $EO_{12}SO_{10}$ and $EO_{10}SO_{10}EO_{10}$ copolymers, only two regions are observed in their adsorption isotherms as a consequence of their low molecular weight, short SO and EO block lengths, and much larger SO/EO ratio. The latter involves the disappearance of the pseudoplateau region due to the decrease in the fractional interfacial area occupied by EO segments. Finally, surface circular micelles are observed by AFM pictures at two surface transfer pressures. A decrease in micelle size and an increase in monolayer thickness are observed with an increase in transfer pressure. In addition, at the largest transfer pressure, elongated micelles are observed. In the case of copolymer $EO_{12}SO_{10}$, association of micelles is also observed. Aggregation numbers derived from AFM images increase with the increase of the SO weight fraction at a certain deposition pressure, which can be a consequence of stronger attractive interactions between the SO blocks to avoid contact with the solvent. The lower aggregation number of copolymer $EO_{137}SO_{18}EO_{137}$ may arise from the steric repulsion of EO chains at the interface due to the longer PEO blocks if compared to the other block copolymer.

Acknowledgment. The authors thank the Ministerio de Ciencia e Innovación (MICINN) for research projects MAT 2007-6107 and Xunta de Galicia for additional financial support under project INCITE09206020PR. S.G.-L. thanks the MICINN for her FPI scholarship. The authors also thank Prof. D. Attwood and C. Booth for the generous gift of the copolymers.

Supporting Information Available: Size and height distributions of aggregates formed in Langmuir−Blodgett films of copolymers at surface pressures of 5 and 11 mN/M. This material is available free of charge via the Internet at http://pubs.acs.org.

References and Notes

(1) Edens, M. W. *Nonionic Surfactants, Polyoxyalkylene Block Copolymers*; Marcel Dekker: New York, 1996.
(2) Riess, G.; Cheymol, A.; Hoerner, P.; Krikorian, R. *Adv. Colloid Interface Sci.* **2004**, *108*−*109*, 43–48.
(3) Tao, Y.; Ma, B.; Segalman, R. A. *Macromolecules* **2008**, *41*, 7152–7159.
(4) Boudier, A.; Aubert-Pouëssel, A.; Gérardin, C.; Devoisselle, J. M.; Bégu, S. *Int. J. Pharm.* **2009**, *379*, 212–217.
(5) Gilcreest, V. P.; Dawson, K. A.; Gorelov, A. V. *J. Phys. Chem. B* **2006**, *110*, 21903–21910.
(6) George, P. A.; Donose, B. C.; Cooper-White, J. J. *Biomaterials* **2009**, *30*, 2449–2456.
(7) Sedev, R.; Jachimska, B.; Khristov, K.; Malysa, K.; Exrowa, D. *J. Dispersion Sci. Technol.* **1999**, *20*, 1759–1776.
(8) Alexandridis, P.; Lindman, B. *Amphiphilic Block Copolymers: Self-Assembly and Applications*; Elsevier Science: Amsterdam, 2000.
(9) Park, S.; Wang, J. W.; Kim, B.; Russell, T. P. *Nano Lett.* **2008**, *8*, 1667–1672.
(10) Park, S.; Kim, B.; Wang, J. W.; Russell, T. P. *Adv. Mater.* **2008**, *20*, 681–685.
(11) Hillmyer, H. A. *Adv. Polym. Sci.* **2005**, *190*, 137.
(12) Crothers, M.; Attwood, D.; Collet, J. H.; Yang, Z.; Booth, C.; Taboada, P.; Mosquera, V.; Ricardo, N. P. S.; Martini, L. G. A. *Langmuir* **2002**, *18*, 8685–8691.
(13) Yang, Z. M.; Crothers, M.; Ricardo, N. P. S.; Chaibundit, C.; Taboada, P.; Mosquera, V.; Kelarakis, A.; Havredaki, V.; Martini, L.; Valder, C.; Collett, J. H.; Attwood, D.; Heatley, F.; Booth, C. *Langmuir* **2003**, *19*, 943–950.
(14) Booth, C.; Attwood, D.; Price, C. *Phys. Chem. Chem. Phys.* **2006**, *8*, 3612–3622.
(15) Riess, G. *Prog. Polym. Sci.* **2003**, *28*, 1107–1170.
(16) Booth, C.; Attwood, D. *Macromol. Rapid Commun.* **2000**, *21*, 501–527.
(17) Gangaly, R.; Awal, V. K.; Hassan, P. A. *J. Colloid Interface Sci.* **2007**, *325*, 693–700.
(18) Battaglia, G.; Ryan, A. J. *J. Am. Chem. Soc.* **2005**, *127*, 8757–8764.
(19) Bryskhe, K.; Jansson, J.; Topgaard, D.; Schillén., K.; Olsson, U. *J. Phys. Chem. B* **2004**, *108*, 9710–9719.
(20) Chaibundit, C.; Sumanatrakool, P.; Chinchew, S.; Kanatharana, P.; Tattershall, C. E.; Booth, C.; Yuan, Y.-F. *J. Colloid Interface Sci.* **2005**, *283*, 544–554.
(21) Barbosa, S.; Cheema, M. A.; Taboada, P.; Mosquera, V. *J. Phys. Chem. B* **2007**, *111*, 10920–10928.
(22) Vaughn, T. G.; suter, H. R.; Lunsted, L. G.; Kramer, M. G. *J. Am. Oil Chem. Soc.* **1951**, *28*, 294.
(23) Nace, V. M. *J. Am. Oil Chem. Soc.* **1996**, *73*, 1–8.

(24) Fleute-Schlachter, I. Goldschmidt Industrial Specialties, Essen, Germany. Private communication.
(25) O′Connor, S. M.; Gehrke, S. H.; Retzinger, G. S. *Langmuir* **1999**, *15*, 2580–2585.
(26) Rippner Blomquist, B.; Wärnheim, T.; Claesson, P. M. *Langmuir* **2005**, *21*, 6373–6384.
(27) González-López, J.; Sandez-Macho, I.; Concheiro, A.; Alvarez-Lorenzo, C. *J. Phys. Chem. C* **2010**, *114*, 1181–1189.
(28) González-López, J.; Alvarez-Lorenzo, C.; Taboada, P.; Sosnik, A.; Sandez-Macho, I.; Concheiro, A. *Langmuir* **2008**, *24*, 10688–10697.
(29) Hodges, C. S.; Neville, F.; Konovalov, O.; Hammond, R. B.; Gidalevitz, D.; Hamley, I. W. *Langmuir* **2006**, *22*, 8821–8825.
(30) Ricardo, N. M. P. S.; Chaibundit, C.; Yang, Z.; Attwood, D.; Booth, C. *Langmuir* **2006**, *22*, 1301–1306.
(31) Pinho, M. E. N.; Costa, F. M. L. L.; Filho, F. B. S.; Ricardo, N. M. P. S.; Yeates, S. G.; Attwood, D.; Booth, C. *Int. J. Pharm.* **2007**, *328*, 95–98.
(32) Juárez, J.; Taboada, P.; Valdez, M. A.; Mosquera, V. *Langmuir* **2008**, *24*, 7107–7116.
(33) Cheyne, R. B.; Moffitt, M. G. *Langmuir* **2005**, *21*, 5453–5460.
(34) Deschênes, L.; Bousmina, M.; Ritcey, A. M. *Langmuir* **2008**, *24*, 3699–3708.
(35) Crothers, M.; Zhou, Z.; Ricardo, N. P. S.; Yang, Z.; Taboada, P.; Chaibundit, C.; Attwood, D.; Booth, C. *Int. J. Pharm.* **2005**, *293*, 91–100.
(36) Elsabahy, M.; Perron, M.-È.; Bertrand, N.; Yu, G.-e.; Leroux, J.-C. *Biomacromolecules* **2007**, *8*, 2250–2257.
(37) Babak, V. G.; Boury, F. *Colloids Surf., A* **2004**, *243*, 33–42.
(38) Babak, V. G.; Baros, F.; Boury, F.; Desbrières, J. *Colloids Surf., B* **2008**, *65*, 43–49.
(39) Ward, A. F. H.; Tordai, L. *J. Chem. Phys.* **1946**, *14*, 453–458.
(40) Hansen, F. K.; Myrvold, R. *J. Colloid Interface Sci.* **1995**, *176*, 498.
(41) Myrvold, R.; Hansen, F. K.; Balinov, B. *Colloids Surf., A* **1996**, *18*, 453.
(42) Muñoz, M. G.; Monroy, F.; Ortega, F.; Rubio, R. G.; Langevin, D. *Langmuir* **2000**, *16*, 1094–1101.
(43) Joos, P.; Fainerman, V. B. *Dynamic Surface Phenomena*; VSP: Utrecht, The Netherlands, 1999.
(44) Kopperud, H. B. M.; Hansen, F. K. *Macromolecules* **2001**, *34*, 5635–5643.
(45) Leiva, A.; Farias, A.; Gargallo, L.; Radic, D. *Eur. Polym. J.* **2008**, *44*, 2589–2598.
(46) Haefele, T.; Kita-Tokarczyk, K.; Meier, W. *Langmuir* **2006**, *22*, 1164–1172.
(47) Kiss, E.; Keszthelyi, T.; Kormany, G.; Hakkel, O. *Macromolecules* **2006**, *39*, 9375–9384.
(48) Elbolk, T. A.; Detellier, C. *J. Phys. Chem. Solids.* **2006**, *67*, 950–955.
(49) Hann, R. A. *Molecular Structure and Monolayer Properties. In Langmuir-Blodgett Films*; Roberts, G., Ed.; Plenum Press: New York, 1990; pp 18−23.
(50) Nivaggioli, T.; Tsao, B.; Alexandridis, P.; Hatton, A. T. *Langmuir* **1995**, *11*, 119–126.
(51) Chen, C.; Even, M. A.; Chen, Z. *Macromolecules* **2003**, *36*, 4478–4484.
(52) Chang, L.-C.; Lin, C. Y.; Kuo, M.-W.; Gau, C.-S. *J. Colloid Interface Sci.* **2005**, *285*, 640–652.
(53) Chang, L. C.; Chang, Y. Y.; Gau, C. S. *J. Colloid Interface Sci.* **2008**, *322*, 263–273.
(54) des Cloizeaux, J. *J. Phys. (Paris)* **1975**, *36*, 281–291.
(55) Vilanove, R.; Rondelez, F. *Phys. Rev. Lett.* **1980**, *45*, 1502.
(56) Faure, M. C.; Bassereau, P.; Lee, L. T.; Menelle, A.; Lheveder, C. *Macromolecules* **1999**, *32*, 8538–8550.
(57) Goncalves da Silva, A. M.; Simoes Gamboa, A. L.; Matinho, J. M. *Langmuir* **1998**, *14*, 5327–5330.
(58) Baker, S. M.; Leach, K. A.; Devereaux, C. E.; Gragson, D. E. *Macromolecules* **2000**, *33*, 5432–5436.
(59) Cox, J. K.; Yu, K.; Constantine, B.; Eisenberg, A.; Lennox, R. B. *Langmuir* **1999**, *15*, 7714–7718.
(60) Devereaux, C. A.; Baker, S. M. *Macromolecules* **2002**, *35*, 1921–1927.
(61) Wen, G.; Chung, B.; Chang, T. *Macromol. Rapid Commun.* **2008**, *29*, 1248–1253.

JP1049777